Supramolecular Engineering of Alkylated, Fluorinated, and Mixed Amphiphiles

Rashmi Rashmi, Hooman Hasheminejad, Svenja Herziger, Alireza Mirzaalipour, Abhishek K Singh, Roland R. Netz, Christoph Böttcher, Hesam Makki,* Sunil K Sharma,* and Rainer Haag*

The rational design of perfluorinated amphiphiles to control the supramolecular aggregation in an aqueous medium is still a key challenge for the engineering of supramolecular architectures. Here, the synthesis and physical properties of six novel non-ionic amphiphiles are presented. The effect of mixed alkylated and perfluorinated segments in a single amphiphile is also studied and compared with only alkylated and perfluorinated units. To explore their morphological behavior in an aqueous medium, dynamic light scattering (DLS) and cryogenic transmission electron microscopy/electron microscopy (cryo-TEM/EM) measurements are used. The assembly mechanisms with theoretical investigations are further confirmed, using the Martini model to perform large-scale coarse-grained molecular dynamics simulations. These novel synthesized amphiphiles offer a greater and more systematic understanding of how perfluorinated systems assemble in an aqueous medium and suggest new directions for rational designing of new amphiphilic systems and interpreting their assembly process.

1. Introduction

Understanding the assembly of supramolecular architectures of complex biomacromolecules provides a road map for biomimetic and bioinspired synthetic systems.[1–5] Amphiphilic systems, which bear both hydrophilic and hydrophobic blocks, have been widely explored, as the thermodynamic incompatibility between the two blocks lends them a tendency toward self-assembly, and so offers a wide variety of morphologies including micelles, fibers, nanotubes, and vesicles, and others.[6–14] This range of supramolecular assemblies have paved their way in mimicking various biological systems such as lipids and proteins and suggested various applications in material science, gene technology, and drug delivery.[15–18] However, the understanding of the aggregation and interactions responsible for these assemblies requires systematic studies combined with theoretical simulations.

A detailed study of oligoglycerol-based amphiphilic architecture has been previously reported by our group, with oligoglycerol head groups of different generations [G1–G3] attached to a long alkyl chain have been proven to produce structurally well-defined architectures.[19–22] In addition, the attachment of fluorinated alkyl chains to oligoglycerol head groups was also explored based on the tendency of fluorinated systems to form lower-curvature nanostructures than hydrogenated analogs.[23,24] As the most electronegative element, fluorine alters the C–F bond

R. Rashmi, S. K Sharma
Department of Chemistry
University of Delhi
Delhi 110007, India
E-mail: rashmidahiya3@gmail.com; sk.sharma90@gmail.com

R. Rashmi, A. K Singh, R. Haag
Institut für Chemie und Biochemie
Organische Chemie
Freie Universität Berlin
Takustraße 3, Berlin 14195, Germany
E-mail: haag@chemie.fu-berlin.de

H. Hasheminejad, A. Mirzaalipour, H. Makki
Department of Polymer and Color Engineering
Amirkabir University of Technology, 1591634311
Tehran, Iran
E-mail: hmakki@aut.ac.ir

S. Herziger, C. Böttcher
Forschungszentrum für Elektronenmikroskopie
Institut für Chemie und Biochemie
Freie Universität Berlin
Fabeckstraße 36a, Berlin 14195, Germany

R. R. Netz
Fachbereich Physik
Freie Universität Berlin
Berlin 14195, Germany

ADVANCED
SCIENCE NEWS
www.advancedsciencenews.com

macro-
molecular
Rapid Communications
www.mrc-journal.de
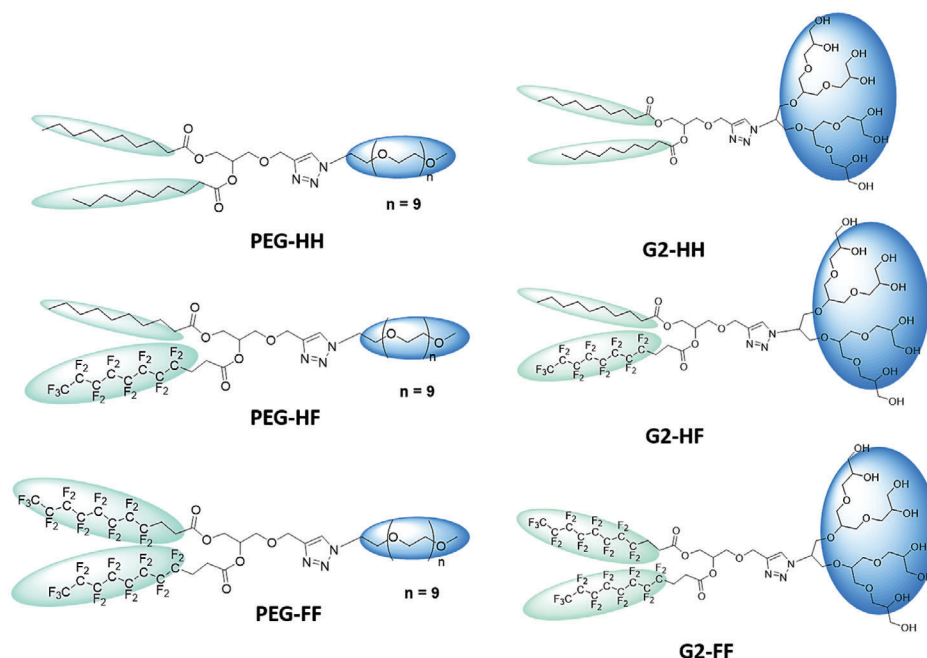
Figure 1. Structural details of the synthesized amphiphiles with a systematic variation of head and tail properties.

polarity by introducing a significant ionic character. Irrespective of the dipole–dipole interaction, perfluoroalkyl chains exhibit strong hydrophobic and lipophobic behavior and dramatically increase the surface activity, thus showing lower aggregation concentration than their hydrogenated counterparts. The per-fluoroalkyl chains' stiffness and the larger cross-sectional area also impart unique properties in terms of the molecular packing parameter as compared to their hydrogenated analogs.[25–28] Perfluoroalkyl-based surfactants and copolymers, besides showing phase behavior, have been reported to self-assemble into varied morphologies such as perforated vesicles, cylindrical micelles, etc.[29–35] The spontaneous formation of perforated vesicles (so-called "stomatosomes") by fluorinated amphiphiles with dendritic head groups[20] motivated the systematic study of the influence of the degree of fluorination, i.e., the number of fluorinated tails, on these compounds' self-assembly behavior, and in particular their assembly morphologies in an aqueous medium. A number of other fluorinated surfactants have been synthesized and explored with single or double chain systems, mixed amphiphiles, or a mixture of fluorinated and hydrogenated systems.[36–39] However, most of the systems explored to date have been ionic; for potential application in biological systems, non-ionic ones are of particular interest, as their pH independency makes them especially useful for hydrophobic drug delivery. We therefore sought to exploit the nonionic supramolecular aggregate structures formed by inducing the effect of mixed alkylated and perfluorinated segments in a single system, as well as to explore other systems with both alkylated and perfluorinated moieties. Moreover, we extended our scope to include a comparison of linear head group geometry as seen with ethylene glycol and dendritic head group geometry, similar to our previous studies with oligoglycerol. Besides morphological aspects, we were interested to understand how fluorination goes along with the concept of spontaneous curvature, e.g., geometri-
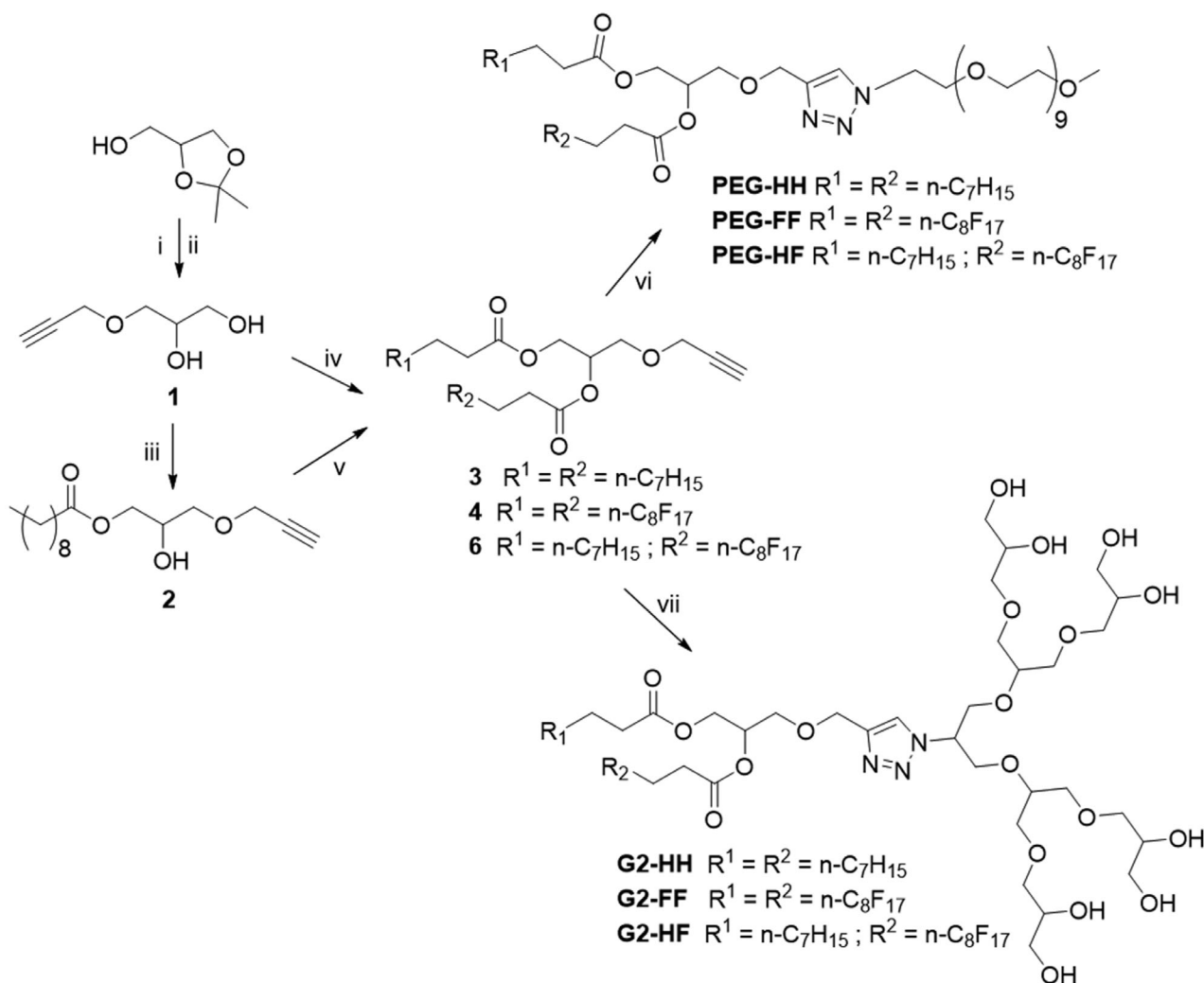
cal asymmetry of the molecule and the principal impact on the assembly behavior. For the systematic study of the two series of amphiphiles, one was synthesized with an ethylene glycol head group [PEG$_{550}$] (**PEG-HH, PEG-HF, PEG-FF**), and the other with a dendritic generation [G2] polyglycerol head group (**G2-HH, G2-HF, G2-FF**) and with perfluorinated octyl chains substituted for one or two alkyl (octyl-) chains (**Figure 1**). Our main tool for investigating the assembly behavior was cryogenic transmission electron microscopy (cryo-TEM), including cryo-electron tomography (cryo-ET). A further theoretical understanding of the assemblies was pursued by using the Martini model to perform large-scale coarse-grained molecular dynamics simulations.

2. Results and Discussion

2.1. Synthesis

For the systematic synthesis of two series of amphiphiles, one with ethylene glycol head groups [PEG$_{550}$] (**PEG-HH, PEG-HF, PEG-FF**) and the other with dendritic polyglycerol [G2] generation (**G2-HH, G2-HF, G2-FF**) head groups, the synthesis was achieved by first synthesizing hydrophobic alkynes of different chains, i.e., alkylated and fluorinated, then mixing the two. The acetal-protected solketal was chosen as a starting material for the synthesis of the hydrophobic alkynes, which were converted to the 3-(prop-2-yn-1-yloxy)propane-1,2-diol (**1**) in two steps (**Scheme 1**) followed by acid coupling with n-decanoic acid and 4,4,5,5,6,6,7,7,8,8,9,9,10,10,11,11,11-heptadecafluoroundecanoic acid by esterification method to synthesize both alkylated and fluorinated alkyne (**3** and **4**).

The synthesis of a monoalkylated product (**2**) proceeded by selective acylation of the primary hydroxyl group of 3-(prop-2-yn-1-yloxy)propane-1,2-diol (**1**) with vinyl ester of decanoic acid using an enzyme-catalyzed trans-esterification re-

ADVANCED
SCIENCE NEWS
www.advancedsciencenews.com

Macro-
molecular
Rapid Communications
www.mrc-journal.de

Scheme 1. Synthesis of targeted amphiphiles: i) Propargyl bromide, NaH, THF, 50 °C, 12 h. ii) DOWEX-50, MeOH, 50 °C, 12 h. iii) Vinyl decanoate, Novozym-435, THF, 35 °C, 6 h. iv) a. *n*-Decanoic acid, EDC. HCl, DMAP, DCM, 35 °C, 24 h; iv) b. 4,4,5,5,6,6,7,7,8,8,9,9,10,10,11,11,11-heptadecafluoroundecanoic acid, EDC. HCl, DMAP, DCM, 35 °C, 24 h. v) 4,4,5,5,6,6,7,7,8,8,9,9,10,10,11,11,11-heptadecafluoroundecanoic acid, EDC. HCl, DMAP, DCM, 35 °C, 24 h. vi) mPEG azide, CuSO$_4$.5H$_2$O, sodium ascorbate, THF:Water (3:1), 35 °C, 24 h. vii) G2 azide, CuSO$_4$.5H$_2$O, sodium ascorbate, THF:Water (3:1), 35 °C, 24 h.

action to yield compound **5**. The acylation reaction occurred exclusively at the primary hydroxyl of compound **1**, leaving its secondary hydroxyl group intact. The monoacylated product (**2**) was then coupled with 4,4,5,5,6,6,7,7,8,8,9,9,10,10,11,11,11-heptadecafluoroundecanoic acid to form a mixed hydrophobic alkyl/fluoro chain (**6**). Reported literature[7] was used for the synthesis of hydrophilic ethylene glycol (PEG-azide) and polyglycerol azides (G2.N$_3$). The synthesized lipophilic propargyl derivatives were then coupled with hydrophilic mPEG/G2-azide through the click approach to synthesize targeted dendronized and PEGylated amphiphiles (Scheme 1).

2.2. Aggregation Behavior

All of the synthesized amphiphiles showed good aqueous solubility and their critical aggregation concentration was measured by fluorescence spectroscopy using Nile red as a probe. The critical aggregation concentration of amphiphilic systems depends more directly on the hydrophobic unit than their hydrophilic content. Due to more hydrophobicity than the hydrogenated alkyl chain, fluorocarbon chains displayed lower aggregation concentration as compared to their hydrogenated counterparts. It has been reported that with respect to aggregation concentration, a CF$_2$ unit brings 1.5 times higher hydrophobicity than a CH$_2$ unit.[39] This empirical rule was found to be in a similar trend in our case also. Amphiphiles with both hydrogenated alkyl chains, i.e., **PEG-HH** and **G2-HH** showed higher concentrations around 3.01×10^{-4} M, however with the replacement of one hydrogenated alkyl chain with a fluorinated chain, the CAC value drops down to 1.09×10^{-4} and 0.92×10^{-4} M for both **PEG-HF** and **G2-HF** respectively. Further, with both fluorinated chain, the amphiphiles **PEG-FF** and **G2-FF** shows much lower critical aggregation concentration in the range 10^{-5} M (**Table 1**). Following the critical ag-

**Table 1.** Structural diversity, DLS, and critical aggregation concentration of the synthesized amphiphiles.

Amphiphile	R_1/R_2 /	DLS size [nm] Number PSD	CAC [M]
PEG-HH	$R_1/R_2 = C_7H_{15}$ / PEG_{550}	10.5	3.01×10^{-4}
PEG-HF	$R_1 = C_7H_{15}$ / $R_2 = C_8F_{17}$ /PEG_{550}	8	1.09×10^{-4}
PEG-FF	$R_1/R_2 = C_8F_{17}$/ PEG_{550}	6.5	7.9×10^{-5}
G2-HH	$R_1/R_2 = C_7H_{15}$/ [G2.0]	10.3	3.0×10^{-4}
G2-HF	$R_1 = C_7H_{15}$ / $R_2 = C_8F_{17}$/[G2.0]	7.8	0.92×10^{-4}
G2-FF	$R_1/R_2 = C_8F_{17}$/ [G2.0]	6.3	0.6×10^{-5}

gregation concentration, the size of the aggregates in an aqueous medium was investigated using dynamic light scattering (DLS), which showed unimodular and bimodular size distribution (Figure SI2, Supporting Information).

2.3. Morphological Investigation (cryo-TEM)

The DLS data reveal the size of aggregation of amphiphile in an aqueous medium, but is not sufficient to determine the morphological behavior of the systems. Cryogenic transmission electron microscopy (cryo-TEM) was therefore performed on all the systems for an in-depth investigation. As most of the amphiphiles showed good aqueous solubility at a concentration of 5×10^{-3} M, except the amphiphile G2-FF, which had a limited solubility of 2.5×10^{-3} M (G2-FF), their aggregation behavior was studied at a concentration of 1×10^{-3} M for all the amphiphiles. The amphiphiles PEG-HH and G2-HH, with their similar hydrophobic units (C-10 alkyl chain) but with different hydrophilic head groups (PEG and polyglycerol, respectively), showed similar morphology: micelles with diameters of 6 nm (PEG-HH) and 7.5 nm (G2-HH) and respective lengths in the range of 10–15 nm. Cryotomography data (surface representation) of different individual micelles in different orientations reveal the morphology of short and twisted strands. The molecular analog with a dendritic head group (G2-HH) shows similar assembly morphology but with larger micellar diameters (7.5 nm). It is known that ethylene glycol heads have a density similar to vitrified water and do not contribute to density in the cryo-TEM images. This is in contrast to dendritic heads, which are clearly visible in cryo-TEM and presumably explain the larger diameter (**Figure 2**).
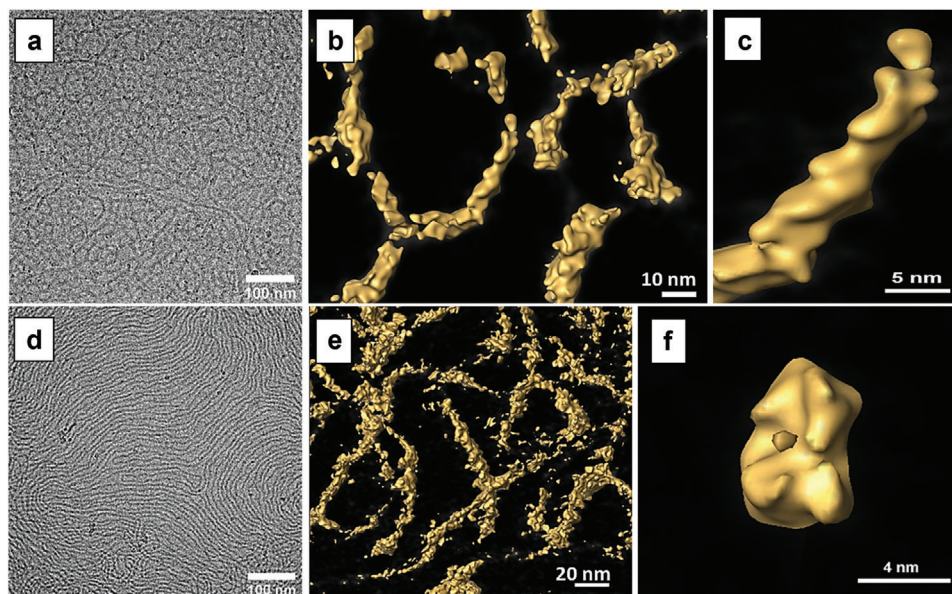
Incorporating a fluoroalkyl chain to form a mixed system of alkyl and fluorine chains changes the morphology from micellar assembly to micellar threads for both PEGylated and polyglycerol-based systems, i.e., PEG-HF and G2-HF, indicating the additional stability offered by the fluoroalkyl chain, which helps in stacking spherical micelles upon one another. From cryo-TEM micrography, the diameter of micellar threads was observed to be ≈6–7 nm (PEG-HF) and 7.5 nm (G2-HF). However, the length of the threads could not be precisely determined, as they formed a network-like structure (**Figure 3**a,d). Cryo-tomography data con-
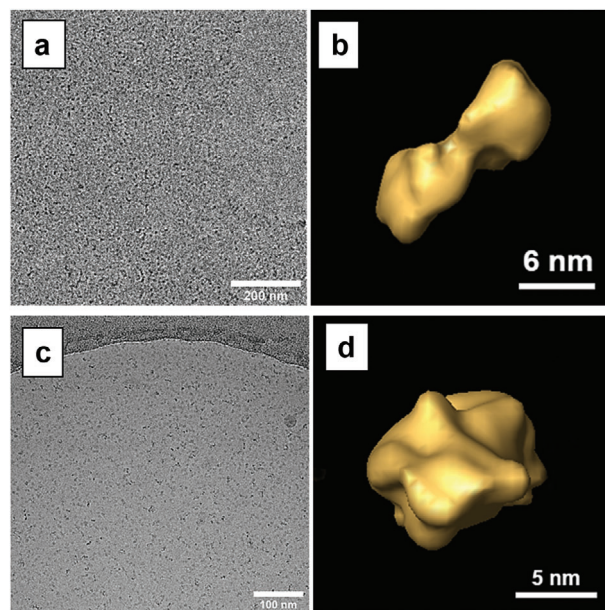
Figure 2. a,c) Cryo-TEM micrographs and b,d) volume reconstructions (surface representations) from cryo-tomography (cryo-ET) data obtained from aqueous amphiphilic solutions. a) Cryo-TEM image of micelles of amphiphile PEG-HH prepared by dissolution. Scale bar: 200 nm. b) Surface representation of a volume reconstructed micelle of PEG-HH. Scale bar: 6 nm. c) Cryo-TEM image of a population of micelles of G2-HH. Scale bar: 100 nm. d) Surface representation of a volume reconstructed micelle G2-HH. Scale bar: 5 nm.

firmed the formation of additional Y junctions. Surface representation of the volume reconstruction indicates a twisted ultrastructure of fibrous strands, very similar to the micelles of PEG-HH and G2-HH. The fourfold motif of the top view (Figure 3f) indicates four subunits for the aggregates, which is similar to those shown in Figure 2d for amphiphiles PEG-HH and G2-HH. The formation of additional Y junctions is further supported by theoretical data that explains the interesting role played by the fluoroalkyl chain in assembly formation (see below).

To study the systematic effect of the fluoroalkyl chain on the amphiphilic systems, amphiphiles PEG-FF and G2-FF with both fluoroalkyl chains were studied, which displayed a clear difference in morphology in both the PEGylated and dendronized cases (**Figure 4**). Amphiphile PEG-FF was observed to form sheet-like structures with various diameters, that is, 30–200 nm. Discoidal patches with different spatial orientations were also observed (Figure 4a). The high-contrast rods in this image represent a side view of the discs and give a thickness of 11 nm, or about four molecular lengths, while the cryo-ET data in Figure 4c reveal the discs as collapsed vesicles where two molecular bilayers are stacked. However, amphiphile G2-FF with a dendronized head group showed wormlike micelles of micrometer length and highly branched networks, where the diameter of all strands was ≈7.5 nm. This networks' morphology (Figure 4d) resembles the previously observed "stomatosomes" structures.[20] The surface representation of the individual strands and strands found in networks (Figure 4e) indicates the twisted supramolecular organization, which is quite regular and defined in some areas.

ADVANCED
SCIENCE NEWS
www.advancedsciencenews.com

[M] acro-
molecular
Rapid Communications
www.mrc-journal.de

Figure 3. a,d) Cryo-TEM images and b,c,e,f) volume reconstructions from cryo-ET data (surface representations) of an aqueous amphiphilic solutions. a) Wormlike micrometer-length micelles of **PEG-HF** prepared by dissolution. Scale bar: 100 nm. b) Central slice of a **PEG-HF** volume reconstruction shows its tendency to form additional Y junctions. Scale bar: 10 nm. c) Surface representation of the volume reconstruction indicates a twisted ultrastructure of fibrous strands of amphiphiles **PEG-HF** prepared by dissolution. Scale bar: 5 nm. d) Wormlike micrometer-length micelles of **G2-HF** prepared by dissolution. Scale bar: 100 nm. e,f) Tomography image of amphiphiles **G2-HF** prepared by dissolution. Scale bar: 20 nm and 4 nm.

2.4. Thermal Behavior

The temperature-dependent cryo-TEM studies were also performed for amphiphile **PEG-FF** at 60 °C, where fibrous assemblies, as well as stomatosomes, were obtained (**Figure 5**a). Branching is clearly visible, but the diameter of the connecting strand varies. Cryo-ET data (Figure 4e) indicates the domination of longer linear assemblies that lie more or less parallel and are connected to the neighboring strands. However, on cooling from 60 °C to ambient temperature, there is a clear tendency toward the recovery of the disclike structures observed before heating. Holes in the stomatosomes disappear, and smooth bilayer membranes are formed instead (Figure 5b). Cryo-TEM images of **G2-FF** prepared at 60 °C reveal the typical pattern of stomatosomes as well as micrometer-long fibrous assemblies.

## 2.5. Coarse-Grained Molecular Dynamics Study

We employed Martini-based coarse-grained molecular dynamics simulations to investigate more closely the process of amphiphile self-assembly. To speed up the aggregation time scale, we performed simulations at amphiphile concentrations of 10×10^{-3}, 15×10^{-3}, and 20×10^{-3} M in water, which are slightly higher than the experimental concentrations. As we show below, the average concentration of amphiphiles does not significantly perturb the shapes and sizes of the obtained micelles and should therefore not impede a meaningful comparison with the experimental data. **Figure 6** shows the final-stage snapshots and their interior morphology separately for all concentrations of **PEG-HH** and **G2-FF** amphiphiles as two examples, as well as the numerical trajectory of their largest cluster's growth. The largest cluster at each

time step has been estimated by the method developed by Daura et al.[40] by counting the number of neighboring beads within a 0.7 nm cutoff. As demonstrated in Figure 6, the simulation results show no considerable difference between different concentrations with respect to the final supramolecular shapes and their interior morphology, which are the two key characteristics extracted from the simulations. However, the lower concentrations exhibit smaller cluster sizes within the 2 µs time frame of our simulations, which reflects the longer equilibration times at low concentrations. The numerical analysis of the cluster size also indicates a slower growth rate at lower concentrations. Therefore, since our work is focused on the shape of the aggregates and on their interior morphology, neither of which shows any obvious dependency on concentration, it seems reasonable to compare the results of simulations of 20×10^{-3} M solutions with cryo-TEM and cryo-tomography images of 1×10^{-3} M solutions.

Figure 7 shows a side-by-side comparison between selected clusters from the simulation results (20×10^{-3} M concentration) and the cryo-TEM images. Upon introducing the fluoroalkyl chains to form mixed systems with both alkyl and fluoroalkyl chains, i.e., **PEG-HF** and **G2-HF**, threadlike structures with diameters of ≈5–7 nm become visible in both the cryo-TEM and simulation results. Moreover, our simulations clearly show Y junction shapes in the case of **G2-HF**, a result that agrees perfectly with the experimental results (Figure 7a,b). Moving on to the simulations of the fully fluorinated amphiphiles, the simulated **PEG-FF** showed a tendency to form large patch-like structures with diameters ≈7 nm, while in the case of **G2-FF**, we can see the formation of twisted strands, which are very similar to the corresponding electron tomography images (Figures 7c,d). Furthermore, in Figure 7d3, the growth of the fibrous assemblies of **G2-FF** leads to perforated shapes, which resemble the large
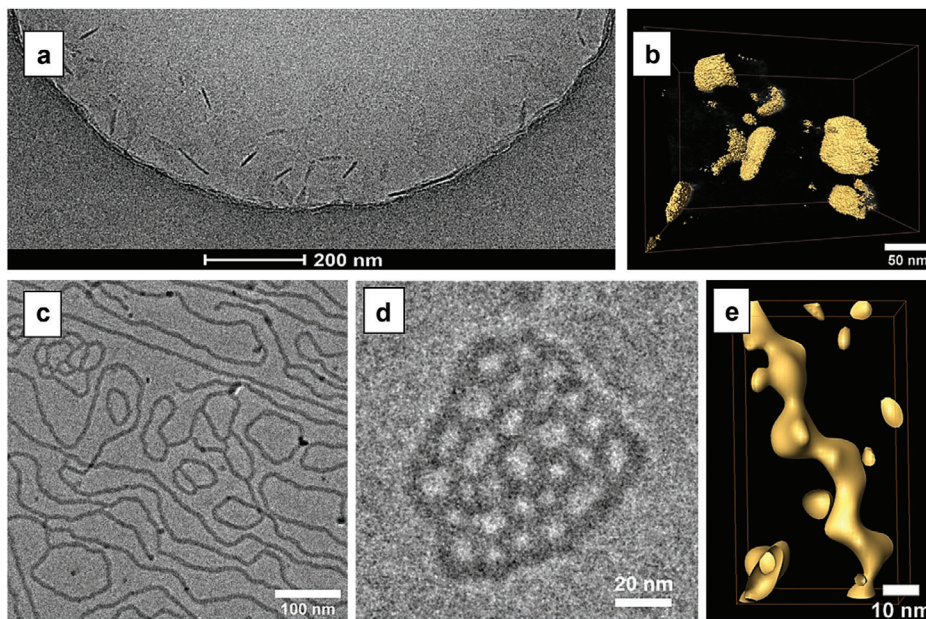
Figure 4. a,c,d) Cryo-TEM images and b,e) volume reconstruction of cryo-ET data (surface representation) b,e) of an aqueous amphiphilic solution of **PEG-FF** and **G2-FF**. a) Discoidal patches in different spatial orientations and b) cryo-ET data reveal the discs as collapsed vesicles composed of two stacked molecular bilayers of amphiphiles **PEG-FF** prepared by dissolution. c,d) Wormlike micelles of micrometer length and highly branched networks were observed for **G2-FF**. e) Corresponding surface representation from cryo-ET data. Scale bars denote a) 200 nm, b) 50 nm, c) 100 nm, d) 20 nm, and e) 10 nm.
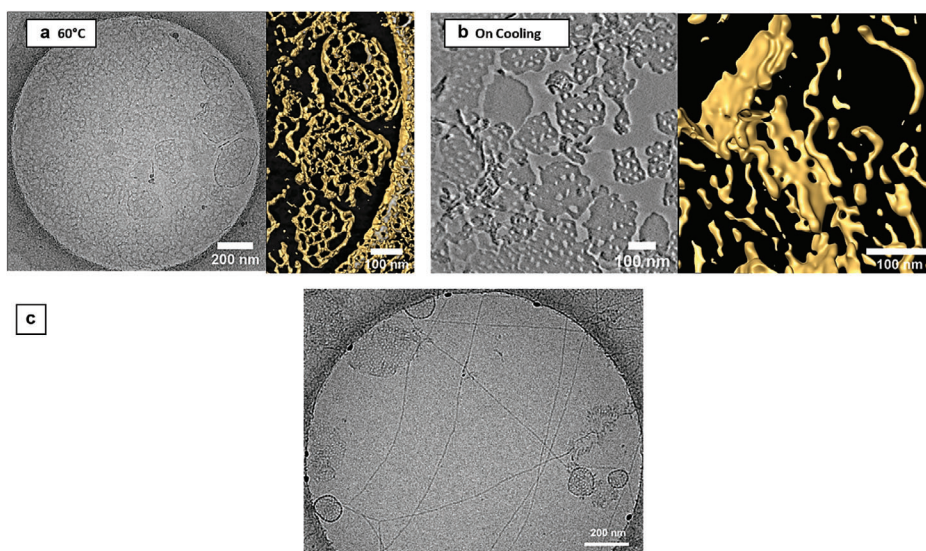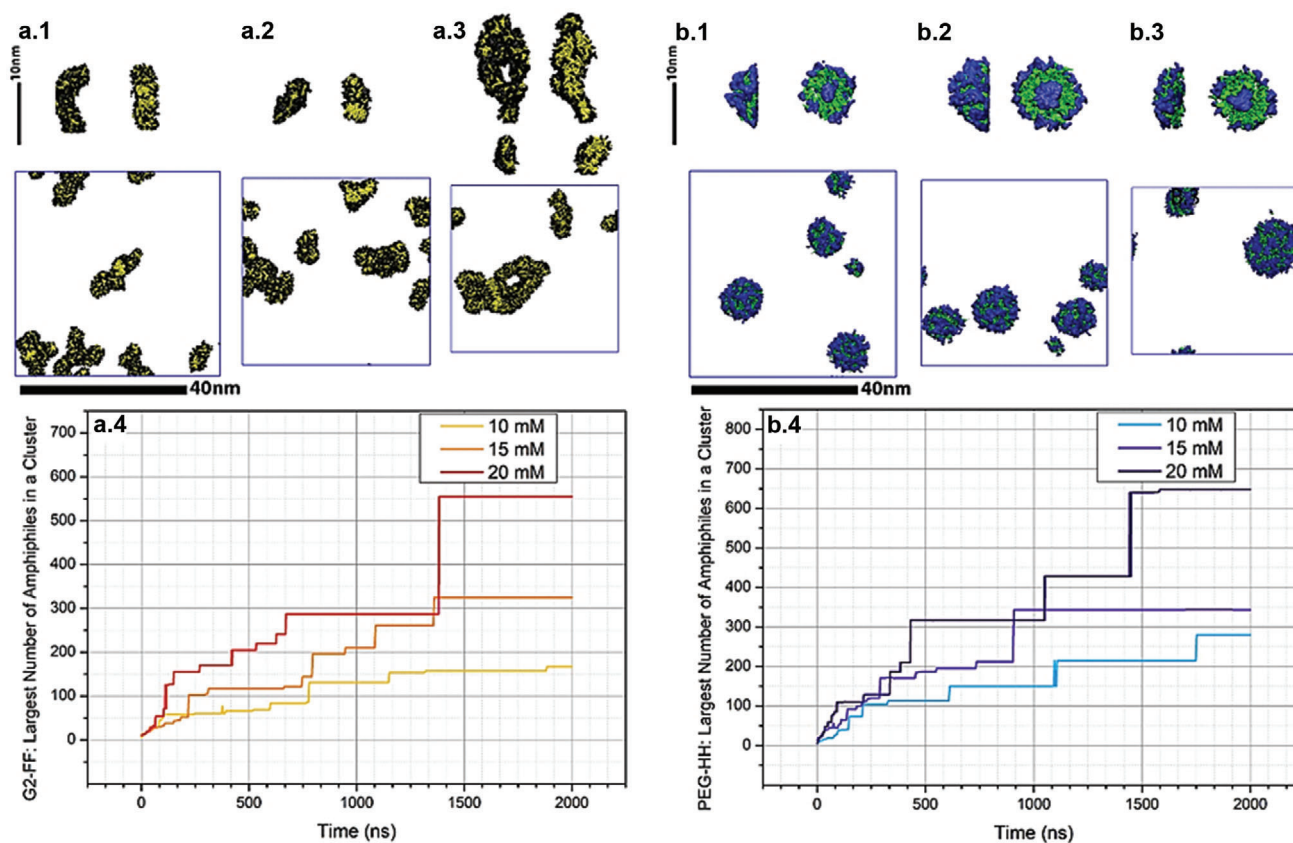

Figure 5. a) Cryo-TEM image of **PEG-FF** prepared in a Vitrobot (Thermo Fisher Scientific) at a chamber temperature of 60 °C, and volume reconstruction in surface representation from cryo-ET data of **PEG-FF**. Scale bar: 200 nm and 100 nm. b) Cryo-TEM image and surface representation of sample **PEG-FF** after cooling from 60 °C to ambient temperature. Scale bar: 100 nm. c) Stomatosome cryo-TEM image of amphiphile **G2-FF** prepared in a Vitrobot at a chamber temperature of 60 °C. Scale bar: 200 nm.

stomatosome structure as observed by cryo-TEM (Figure 7d4). An excellent match is found when comparing the result of this simulation with the cryo-TEM images (Figures 7d4,d5), with pores of 5–10 nm diameter evident in both cases. In fact, in previous theoretical studies of diblock copolymer systems in a selective solvent, perforated lamellar structures have been found to be very slightly free-energetically preferred over non-perforated lamellar structures in the highly swollen limit, which shows that the presence of pores in dilute self-assembled lamellar structures follows a subtle balance of polymer architecture and solvent effects.[41]
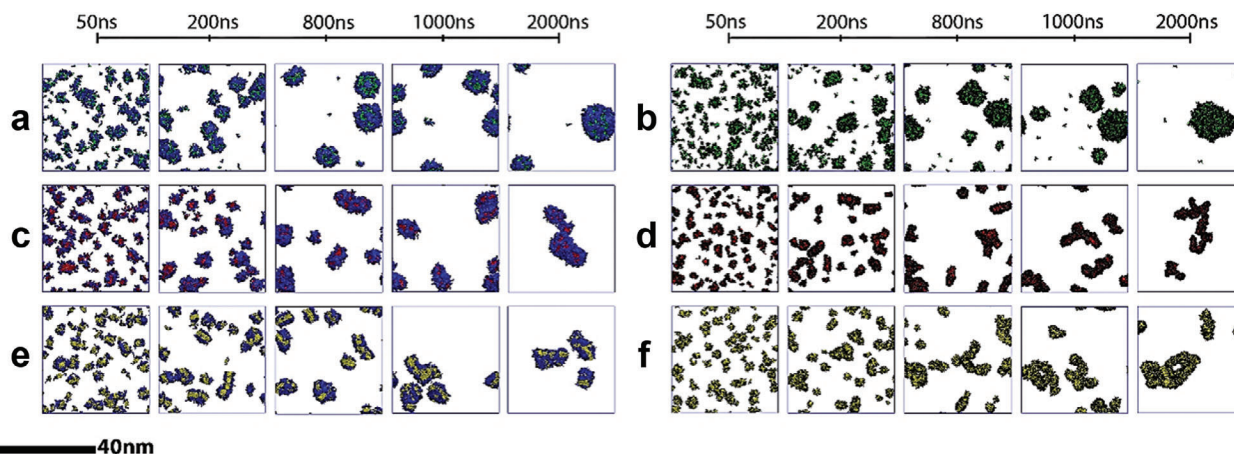
To investigate the effect of replacing alkyl chains with fluorinated ones on the aggregation dynamics, the time evolutions of all simulated amphiphiles were followed. Using the Visual Molecular Dynamics (VMD) software application,[42] snapshots

ADVANCED
SCIENCE NEWS
www.advancedsciencenews.com

{M} acro-
molecular
Rapid Communications
www.mrc-journal.de

Figure 6. Final-stage snapshots of a) **G2-FF** and b) **PEG-HH** simulations with concentrations of 10×10^{-3} (a.1 and b.1), 15×10^{-3} (a.2 and b.2), and 20×10^{-3} M (a.3 and b.3), hydrophobic parts are shown in yellow and green, with hydrophilic parts appearing in black and blue. a.4 and b.4 show the largest cluster size evolution during the simulations.
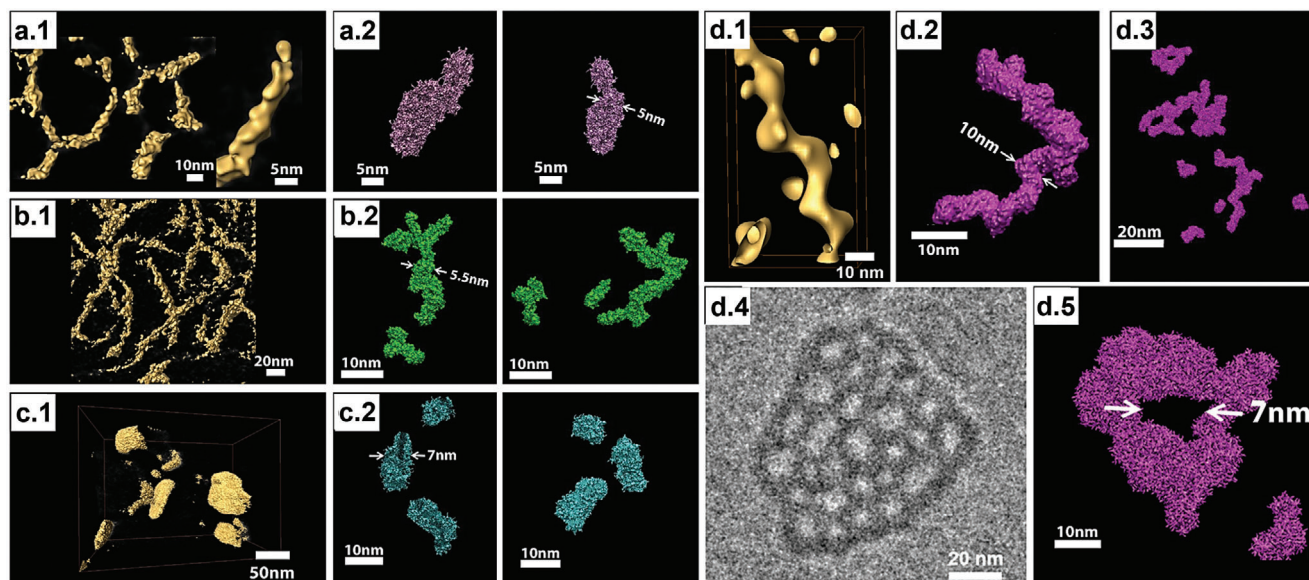
Figure 7. Amphiphile solutions seen in cryo-tomography images (a.1, b.1, c.1, and d.1), Martini simulation images (a.2, b.2, and c.2 with 800 amphiphile molecules, and d.2, d.3, and d.5 with 2500 molecules), and a cryo-TEM image (d.4). All results show striking similarities between the experimental and simulated results. For a) **PEG-HF** and b) **G2-HF**, simulations exhibit thread-shaped aggregates that are connected by Y junctions. c) **PEG-FF** simulations show disclike micelles, while d) **G2-FF** simulations exhibit aggregates with pores that resemble the experimental structures. The pore sizes of **G2-FF** in the cryo-tomography image (d.4) are rather similar to the pore size seen in the 2500 amphiphile simulation (d.2, d.3, and d.5).

ADVANCED
SCIENCE NEWS
www.advancedsciencenews.com

[M] acro-
molecular
Rapid Communications
www.mrc-journal.de

Figure 8. Snapshots of simulations along their evolution for a) **PEG-HH**, b) **G2-HH**, c) **PEG-HF**, d) **G2-HF**, e) **PEG-FF**, and f) **G2-FF**. **PEG-HH** and **G2-HH** grow in a mostly spherical manner (a and b), but upon the replacement of alkyl chains with fluorinated ones, the amphiphiles prefer rodlike aggregations for a certain amount of time before moving on to more complex structures (c3, d2, e2, and f1).

were captured to depict the aggregates' growth from short-diameter micelles to aggregates with nearly 800 amphiphiles. **Figure 8** shows that **PEG-HH** and **G2-HH** clusters kept their spherical/ovoid shapes until the end of the simulations, while the initially spherical clusters of **PEG-HF** and **G2-HF** merged into threads and into more rodlike shapes. Note that in our simulations, the concentrations are larger than in the experiments; this difference might account for the formation of larger spherical or ovoid aggregates in simulated **PEG-HH** and **G2-HH** systems as compared to experimental values. Also, in simulations, the **G2-HF** amphiphiles' tendency to form Y junctions is more pronounced as compared to the experimental results. It is worth mentioning that **PEG-FF** and **G2-FF** aggregates also evolve into wormlike structures, which later fuse into somewhat disc-shaped

clusters in the case of **PEG-FF**, and into more twisted threads for **G2-FF**. The long, twisted threads of **G2-FF** bend over in time and form the perforated structures seen in Figure 8. We capture this interesting phenomenon in a short video of the (2 µs) time evolution of **G2-FF**, which can be found in Supporting Information.

The results demonstrate a nice agreement between the cryo-TEM and coarse-grained molecular dynamics results with respect to the final shapes of the supramolecules. In addition, the simulation trajectories suggest a complex shape evolution during the self-assembly processes of partially and fully fluorinated supramolecules and offer detailed insights into the clusters' interior morphologies by allowing us to slice the aggregates and examine their cross-sectional area. **Figure 9** illustrates simulated side and front views of the cross-sections of **PEG-HF**, **G2-HF**,
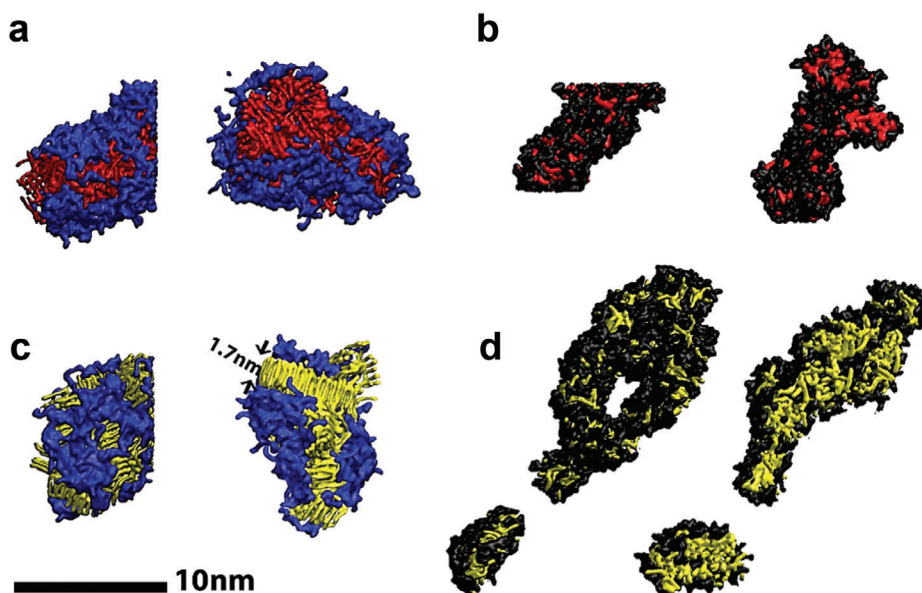
Figure 9. Side and front views of cross-sections from a) **PEG-HF**, b) **G2-HF**, c) **PEG-FF**, and d) **G2-FF** simulations (Red and yellow indicate hydrophobic parts, while black and blue indicate hydrophilic parts.

**ADVANCED
SCIENCE NEWS**

www.advancedsciencenews.com

{M}acro-molecular
Rapid Communications

www.mrc-journal.de

PEG-FF, and **G2-FF**. One can observe a distinct phase separation between the hydrophilic and hydrophobic parts. Moreover, the fully fluorinated amphiphiles show more ordered and crystalline hydrophobic parts as compared to the mixed systems, which most likely is due to the higher stiffness of the fluoroalkyl chains as compared to alkyl ones. For example, in the **PEG-FF** aggregates, the fluoroalkyl hydrophobic tails are tightly stacked in a straight manner producing a thickness that is almost double the length of one hydrophobic tail ($\approx$1.1 nm). This could explain the larger and more stable clusters of fully fluorinated amphiphiles. Simulated fully fluorinated systems also show a tendency to form double-layer stacks, in line with cryo-TEM results; however, larger simulation systems are needed to quantitatively study the formation of fully collapsed vesicles.

3. Conclusion

In conclusion, we successfully designed and synthesized a new series of double-chain PEGylated and dendronized amphiphiles consisting of both hydrogenated and fluorinated alkyl chains, along with a mixture of both in a single system. Most of the systems were found to show good aqueous solubility, and their aggregation behavior was studied using DLS, cryo-TEM, and cryo-EM measurements. From the cryo-TEM data, it was observed that the hydrophilic units, that is, PEG and dendrons, showed not much difference in aggregation behavior, except the **PEG-FF** and **G2-FF** aggregates. As observed by theoretical studies, these aggregates first evolved into wormlike structures, which later fused into somewhat disc-shaped clusters in the case of **PEG-FF**, and more twisted threads for **G2-FF**. An exact explanation of this behavior is not clear, but from theoretical studies, it is observed that in the case of **PEG-FF** aggregates, the fluoroalkyl hydrophobic tails tend to form a bilayer structure with a thickness that is almost double the length of one hydrophobic tail. This could explain the larger, more stable clusters formed by the fully fluorinated amphiphile **PEG-FF**. As reported previously by our group, the flexibility of fluorinated chains changes upon heating the system up to 60 °C, which could explain the clusters' thermal behavior of dissolving into fibrous assemblies and stomatosomes. As expected from our previous studies, **PEG-HH** and **G2-HH**, with their hydrogenated alkyl chains, formed micellar aggregates. However, upon introducing a fluorinated alkyl chain, their assembly morphology shifted to micellar threads with additional Y junctions, which is confirmed by our simulations. This behavior of preferentially stacking themselves upon one another to form threads, rather than just micellar assemblies, may be explained by the fluoroalkyl chain's larger size and higher stiffness, along with high fluorous interaction. These findings offer an increased and more systematic understanding of the assembly of perfluorinated systems in an aqueous medium, paving the way for new opportunities to investigate and interpret this assembly process and utilizing this assembly for further biomedical applications in the future.

4. Experimental Section

All the chemicals and solvents were purchased from Spectrochem Pvt. Ltd., India and Sigma–Aldrich Chemicals, USA. Immobilized *Candida*

antarctica lipase (Novozym 435) was obtained from Novo Nordisk A/S Denmark. The reactions were performed in dried and distilled solvents prior to use. To monitor the progress of the reaction, a pre-coated TLC plate (Merck silica gel 60F254) was used with visualization of the spots on TLC using ceric solution. For column chromatography, silica gel (100–200 mesh) was used. Millipore water was used for the preparation of samples for their physiochemical characterization and transport studies. The ^{1}H and ^{13}C NMR spectra were recorded on JEOL 400 MHz, Bruker DRX 400, and Bruker AMX 500 MHz spectrometers with the residual solvent peak used as a reference. Infrared spectra (IR) of the samples were recorded using a Perkin–Elmer FT-IR model 9 spectrometer. The chemical shift values were on a δ scale, and the coupling constant values (J) were in Hertz. High-resolution mass spectrometry (HRMS) data were recorded on Q-TOF LCMS-Agilent Technology-6530 and HPLC/MS-Agilent 6210 (Agilent Technologies). To obtain the molecular weight of amphiphiles, Waters GPC system equipped with a Waters 515 HPLC pump, refractive index detector, and styragel HR column was used using tetrahydrofuran (THF) as an eluent at a flow rate of 1.2 mL min^{-1} and molecular weight calibration carried using polystyrene standards.

Critical Aggregation Concentration Measurements: The critical aggregation concentration (CAC) of the synthesized amphiphiles was studied by fluorescence technique using "Nile red" as a model dye. A stock solution of the dye of concentration 5 mg mL^{-1} was prepared in THF. Ten microliters of the stock solution was added in each empty vial followed by complete evaporation of THF to form a thin layer. For the preparation of stock solutions of amphiphiles of 1× 10^{-3} M, Milli-Q water was used and allowed to stir for 1 h. To achieve different concentrations of the amphiphiles, twofold serial dilution of the stock solutions was done that was then transferred to the vials having a thin film of the dye followed by overnight stirring. The non-encapsulated dye in all the solutions was removed by filtration through a 0.45 μm polytetrafluoroethylene (PTFE) filter with subsequent fluorescence measurements using Cary Eclipse fluorescence spectrophotometer. The plot of fluorescence intensity maxima values against log [amphiphile concentration] for different samples afforded the CAC value.

Dynamic Light Scattering: Malvern Zetasizer Nano ZS analyzer integrated with 4 mW He-Ne laser, $\lambda = 633$ nm, using backscattering detection (scattering angle $\theta = 173°$) with an avalanche photodiode detector, was used for determining the size of nanostructures (micelles/aggregates) formed by the supramolecular organization of amphiphiles in the aqueous solution (Milli-Q water) at a concentration of 5 mg mL^{-1}. The samples were then further allowed to mix at 25 °C for 20 h with vigorous stirring. The obtained solutions were then filtered through a 0.22 μm PTFE filter and equilibrated for 1 h at room temperature, then transferred to disposable micro BRAND ultraviolet (UV) cuvettes and used for DLS measurements.

Cryo-Sample Preparation: Samples were prepared by use of a Vitrobot Mark IV (Thermo Fisher Scientific). The Vitrobot was operated at 22 °C (or 60 °C where indicated) and at a relative humidity of 100%. In the preparation chamber of the Vitrobot, 4 μL of the corresponding sample solution was applied on a Quantifoil (R4/1 batch of Quantifoil Micro Tools GmbH, Jena, Germany) grid that was surface plasma treated for 60 s at 10 mA just prior to use. The excess sample was removed by blotting for 4 s, and the ultrathin film thus formed was plunged into liquid ethane just above its freezing point.

Cryo-Electron Microscopy (cryo-TEM): Vitrified samples were imaged with a Talos Arctica TEM (Thermo Fisher Scientific, Hillsboro, Oregon; USA) at 200 kV accelerating voltage employing a Volta phase plate in the back focal plane of the objective lens at a primary magnification of 28k. Images were recorded by a Falcon III direct electron detector at full 4k resolution resulting in a pixel size of 0.373 nm per pixel. The defocus value was set to −300 nm.

Cryo-Electron Tomography (cryo-ET): Vitrified samples were transferred under liquid nitrogen into a Talos Arctica TEM (Thermo Fisher Scientific, Hillsboro, Oregon; USA) at 200 kV accelerating voltage employing a Volta phase plate in the back focal plane of the objective lens at a primary magnification of 28 000×. Image series in the tilt range of −64°/64° (2° tilt-increments) were recorded by a Falcon III direct electron detector at full 4k resolution resulting in a pixel size of 0.373 nm per pixel. The defocus value was set to −300 nm.

**ADVANCED
SCIENCE NEWS**

www.advancedsciencenews.com

{M acro-
molecular
Rapid Communications

www.mrc-journal.de

Data Processing: Image stack alignment and 3D reconstruction were performed in the context of the FEI Inspect 3D software V4.1. Visualization in Voltex, as well as surface representation, was done by the use of AMIRA software Version 6.0 (Thermo Fisher Scientific, Hillsboro, Oregon; USA).

Coarse-Grained Molecular Dynamics Simulations: CHARMM force field[43,44] was employed for the all-atom stage of the simulations as a validated reference to compare the coarse-grained results as well as the starting point to map the coarse-grained structures on. The recently released Martini 3 force field was used,[45] which had been significantly improved with respect to the interaction balances, new bead types, and expanded ability to include specific interactions as compared to the previous versions. A nice agreement between the properties of all-atom and coarse-grained structures was seen, see Supporting Information, where comprehensive sections on coarse-graining, parametrization, and validations were provided.

All-atom and coarse-grained simulations were carried out using the GROMACS software.[46] Simulation boxes of 800 amphiphile molecules in water with concentrations of 20×10^{-3}, 15×10^{-3}, and 10×10^{-3} M were made. A box of 2500 amphiphiles with 20×10^{-3} M concentration was also made only in the case of G2-FF to make a clearer visualization of its perforated structure, as seen in the cryo-TEM images. After energy minimization, NVT and NPT simulations were conducted in 300 K and 1 bar by employing the Berendsen thermostat in the velocity rescaling scheme,[47] and Parrinello–Rahman barostat,[48,49] respectively. The production runs were 2 µs long under the NPT ensemble.

Supporting Information

Supporting Information is available from the Wiley Online Library or from the author.

Conflict of Interest

The authors declare no conflict of interest.

Data Availability Statement

The data that support the findings of this study are available in the supplementary material of this article.

[1] P. Ghosh, N. Fridman, G. Maayan, *Chem. – A Eur. J.* **2021**, *27*, 634.
[2] Z. Lei, P. Wu, *Nat. Commun.* **2018**, *9*, 1134.
[3] A. Mishra, D. B. Korlepara, M. Kumar, A. Jain, N. Jonnalagadda, K. K. Bejagam, S. Balasubramanian, S. J. George, *Nat. Commun.* **2018**, *9*, 2510.
[4] D. Ahmadi, R. Ledder, N. Mahmoudi, P. Li, J. Tellam, D. Robinson, R. K. Heenan, P. Smith, C. D. Lorenz, D. J. Barlow, M. J. Lawrence, *J. Colloid Interface Sci.* **2021**, *587*, 597.
[5] J. M. Korde, B. Kandasubramanian, *Chem. Eng. J.* **2020**, *379*, 122430.
[6] A. K. Singh, B. N. S. Thota, B. Schade, K. Achazi, A. Khan, C. Böttcher, S. K. Sharma, R. Haag, *Chem. – An Asian J* **2017**, *12*, 1796.
[7] R. Rashmi, A. K. Singh, K. Achazi, B. Schade, C. Böttcher, R. Haag, S. K. Sharma, *RSC Adv.* **2018**, *8*, 31777.
[8] Rashmi, F. Zabihi, A. K. Singh, K. Achazi, B. Schade, S. Hedtrich, R. Haag, S. K. Sharma, *Int. J. Pharm.* **2020**, *580*, 119212.
[9] Rashmi, A. K. Singh, K. Achazi, S. Ehrmann, C. Böttcher, R. Haag, S. K. Sharma, *Polym. Chem.* **2020**, *11*, 6772.
[10] Y. Chen, H. X. Gan, Y. W. Tong, *Macromolecules* **2015**, *48*, 2647.
[11] C. Wang, Z. Wang, X.i Zhang, *Acc. Chem. Res.* **2012**, *45*, 608.
[12] J. N. Israelachvili, D. J. Mitchell, B. W. Ninham, *J. Chem. Soc. Faraday Trans. 2 Mol. Chem. Phys.* **1976**, *72*, 1525.
[13] G. Wang, B. Tang, Y. Liu, Q. Gao, Z. Wang, X.i Zhang, *Chem. Sci.* **2016**, *7*, 1151.
[14] M. P. Hendricks, K. Sato, L. C. Palmer, S. I. Stupp, *Acc. Chem. Res.* **2017**, *50*, 2440.
[15] A. S. Knight, J. Larsson, J. M. Ren, R. Bou Zerdan, S. Seguin, R. Vrahas, J. Liu, G. Ren, C. J. Hawker, *J. Am. Chem. Soc.* **2018**, *140*, 1409.
[16] J. Wang, X. Wang, F. Yang, H. Shen, Y. You, D. Wu, *Langmuir* **2015**, *31*, 13834.
[17] Z. Song, X. Chen, X. You, K. Huang, A. Dhinakar, Z. Gu, J. Wu, *Biomater. Sci.* **2017**, *5*, 2369.
[18] C. Xie, X.u Zhen, Q. Lei, R. Ni, K. Pu, *Adv. Funct. Mater.* **2017**, *27*, 1605397.
[19] S. Kumar, K. Ludwig, B. Schade, H. Von Berlepsch, I. Papp, R. Tyagi, M. Gulia, R. Haag, C. Böttcher, *Chem. – A Eur. J.* **2016**, *22*, 5629.
[20] H. V. Berlepsch, B. N. S. Thota, M. Wyszogrodzka, S. De Carlo, R. Haag, C. Bö, *Soft Matter* **2018**, *14*, 5256.
[21] B. N. S. Thota, L. H. Urner, R. Haag, *Chem. Rev.* **2016**, *116*, 2079.
[22] B. Trappmann, K. Ludwig, M. R. Radowski, A. Shukla, A. Mohr, H. Rehage, C. Böttcher, R. Haag, *J. Am. Chem. Soc.* **2010**, *132*, 11119.
[23] O. Wagner, B. N. S. Thota, B. Schade, F. Neumann, J. L. Cuellar, C. Böttcher, R. Haag, *Polym. Chem* **2016**, *7*, 2222.
[24] O. Wagner, M. Zieringer, W. J. Duncanson, D. A. Weitz, R. Haag, *Int. J. Mol. Sci.* **2015**, *16*, 20184.
[25] M. P. Krafft, J. G. Riess, *Biochimie* **1998**, *80*, 489.
[26] M. Krafft, *Curr. Opin. Colloid Interface Sci.* **2003**, *8*, 243.
[27] H. Omorodion, B. Twamley, J. A. Platts, R. J. Baker, *Cryst. Growth Des.* **2015**, *15*, 2835.
[28] S. Shin, N. Collazo, S. A. Rice, *J. Chem. Phys.* **1992**, *96*, 1352.
[29] M. Yamanaka, K. Sada, M. Miyata, K. Hanabusa, K. Nakano, *Chem. Commun.* **2006**, 2248.
[30] T. Shimoaka, H. Ukai, K. Kurishima, K. Takei, N. Yamada, T. Hasegawa, *J. Phys. Chem. C* **2018**, *122*, 22018.
[31] F. Petit, I. Iliopoulos, R. Audebert, S. Szönyi, *Langmuir* **1997**, *13*, 4229.
[32] H. Tamiaki, T. Nishiyama, R. Shibata, *Bioorganic Med. Chem. Lett.* **2007**, *17*, 1920.
[33] R. Kise, A. Fukumi, N. Shioya, T. Shimoaka, M. Sonoyama, H. Amii, T. Takagi, T. Kanamori, K. Eda, T. Hasegawa, *Bull. Chem. Soc. Jpn.* **2019**, *92*, 785.
[34] T. Maekawa, S. Kamata, M. Matsuo, *J. Fluor. Chem.* **1991**, *54*, 84.
[35] L. Zhang, S. Lin, Q. Tong, Y. Li, Y. Wang, Y.i Li, B. Li, Y. Yang, *Chirality* **2019**, *31*, 992.
[36] P. Kekicheff, G. J. T. Tiddy, *J. Phys. Chem.* **1989**, *93*, 2520.
[37] Y. Chaudier, P. Barthélémy, B. Pucci, *Tetrahedron Lett.* **2001**, *42*, 3583.
[38] K. Matsuoka, *Curr. Opin. Colloid Interface Sci.* **2003**, *8*, 227.
[39] R. Odax, I. Huc, D. Danino, Y. Talmon, *Langmuir* **2000**, *16*, 9759.

[40] X. Daura, K. Gademann, B. Jaun, D. Seebach, W. F. Van Gunsteren, A. E. Mark, *Angew. Chem., Int. Ed.* **1999**, *38*, 236.

[41] R. R. Netz, M. Schick, *Phys. Rev. E* **1996**, *53*, 3875.

[42] W. Humphrey, A. Dalke, K. Schulten, *J. Molec. Graphics* **1996**, *14*, 33.

[43] B. R. Brooks, C. L. Brooks, III, A. D. Mackerell, L. Nilsson, R. J. Petrella, B. Roux, Y. Won, G. Archontis, C. Bartels, S. Boresch, A. Caflisch, L. Caves, Q. Cui, A. R. Dinner, M. Feig, S. Fischer, J. Gao, M. Hodoscek, W. Im, K. Kuczera, T. Lazaridis, J. Ma, V. Ovchinnikov, E. Paci, R. W. Pastor, C. B. Post, J. Z. Pu, M. Schaefer, B. Tidor, R. M. Venable, et al., *J. Comp. Chem.* **2009**, *30*, 1545.

[44] S. Jo, T. Kim, V. G. Iyer, W. Im, *J. Comput. Chem.* **2008**, *29*, 1859.

[45] P. C. T. Souza, R. Alessandri, J. Barnoud, S. Thallmair, I. Faustino, F. Grünewald, I. Patmanidis, H. Abdizadeh, B. M. H. Bruininks, T. A. Wassenaar, P. C. Kroon, J. Melcr, V. Nieto, V. Corradi, H. M. Khan, J. Domański, M. Javanainen, H. Martinez-Seara, N. Reuter, R. B. Best, I. Vattulainen, L. Monticelli, X. Periole, D. P. Tieleman, A. H. de Vries, S. J. Marrink, *Nat. Methods* **2021**, *18*, 382.

[46] Lindahl, Abraham, Hess, van der Spoel, *GROMACS Documentation*, **2021**.

[47] G. Bussi, D. Donadio, Parrinello, *J. Chem. Phys.* **2007**, *126*, 014101.

[48] M. Parrinello, A. Rahman, *J. Appl. Phys* **1981**, *52*, 7182.

[49] S. Nosé, M. L. Klein, *Mol. Phys.* **1983**, *50*, 1055.